Numerical Study of Crystal Growth in Reaction-Diffusion Systems using Front Tracking

Saurabh Joglekar and Xiaolin Li

Abstract We study the crystal growth in a Reaction-Diffusion System for the generic reaction $A + B \longrightarrow C$. Reactants A and B react to form the product C which then undergoes phase transition. We have used the Lagrangian Front Tracking to explicitly track the crystal surface. The evolution of the concentrations of A, B and C is described by a system of three partial differential equations. This system is solved using finite difference method. Main focus of the study is on observing the effects of different parameters on the crystal growth, namely the diffusion coefficients, homogeneous reaction constant, heterogeneous reaction constant and the equilibrium concentration.

Key words: Reaction-Diffusion Equations, Crystal Growth, Lagrangian Front Tracking

1 Introduction

Xiaolin Li et al [1] have studied a single component Reaction-Diffusion system through front tracking without consideration of advection, in which the reaction term is replaced by precipitation term at the fluid-solid interface. The governing equations for the solute concentration $C = C(\vec{x},t)$ are as follows:

$$\frac{\partial C}{\partial t} = D\nabla^2 C, \qquad \text{for } \vec{x} \in \Omega \tag{1}$$

Here Ω is the ambient region containing solute and D is diffusion coefficient. At the fluid-solid interface $\partial\Omega$, the front growth is governed by:

Saurabh Joglekar and Xiaolin Li
Dept. of Applied Mathematics and Statistics, Stony Brook University, Stony Brook, NY 11794-3600, USA
e-mail: saurabh.joglekar@gmail.com, e-mail: xiaolin.li@stonybrook.edu

$$D\frac{dC}{dn}(\vec{x_s}) = k(C(\vec{x_s}) - C_e) \tag{2}$$

where k is the reaction rate per unit area for the solute from the liquid phase to precipitate onto the solid phase at the interface, C_e is the equilibrium concentration and $C(\vec{x_s})$ is the local concentration of solute at the interface. Interface is propagated with the normal velocity,

$$v_n = \frac{D}{\rho_s}\frac{dC}{dn}(\vec{x_s}) \tag{3}$$

where ρ_s is the density of solid phase. Interface growth and the dendritic structure of the precipitate have been studied at different Damkohler numbers. Front tracking is well suited to dendritic structures at large Damkohler numbers where high resolution is necessary.

Tartakovsky et al [3] have studied multi-component Reaction-Diffusion systems for the chemical reaction $A + B \longrightarrow C_{(aq\,+\,solid)}$, on two different spatial scales, Pore-scale and Darcy-scale. Smoothed particle hydrodynamics (SPH) has been applied to carry out hybrid simulations on two different spatial scales. Let $A(\vec{x},t)$, $B(\vec{x},t)$, $C(\vec{x},t)$ and D_a, D_b, D_c be the concentrations and diffusion coefficients of components A, B and C in solute phase. Let k and k_{AB} be heterogeneous and homogeneous reaction rates, and ρ_s be the density of solid phase. Then the Pore scale model satisfies following system of equations:

$$\frac{\partial A}{\partial t} = \nabla\cdot(D_a\nabla A) - k_{AB}AB \tag{4}$$

$$\frac{\partial B}{\partial t} = \nabla\cdot(D_b\nabla B) - k_{AB}AB \tag{5}$$

$$\frac{\partial C}{\partial t} = \nabla\cdot(D_c\nabla C) + k_{AB}AB - k\int_F H(C-C_{eq})\delta(\vec{x}-\vec{x}_f)d\vec{x}_f \tag{6}$$

where $H(x)$ is the Heaviside step function and the integration is taken over the whole fluid-solid interface. Soluble precipitate C follows the first order kinetic reaction model on the fluid-solid interface,

$$D_c\frac{dC}{dn} = k(C - C_{eq}) \tag{7}$$

The interface advances into the liquid with normal velocity,

$$v_n(\vec{x_s}) = \frac{D_c}{\rho_s}\nabla C\cdot\vec{n} \tag{8}$$

Simulations start with a crystal seed already present in the domain. Hence, although the same equations govern the formation of Liesegang Patterns, nucleation theories have not been considered in Tartakovsky et al [3].

2 Front Tracking

The "Front" is defined as the boundary point between two regions containing a sharp discontinuity of a physical variable, e.g. density, concentration, viscocity etc. Theoretically, the function representing the physical variable is not differentiable at a point of discontinuity. This problem can be handled by using the integral form of the governing equations. However, if the numerical scheme is of low order, then the front diffuses quickly losing its sharpness. On the other hand, a high order numerical scheme may cause numerical oscillations near the front and reduce the high order of accuracy near the region[40]. To solve these diffculties, there exist two main strategies, namely front-capturing and front-tracking.

The main idea of front capturing is to use a high order scheme and use artificial viscosity around the front to diffuse it slightly to avoid oscillations. Front capturing works well for shocks but does not work very well for contact discontinuities[40]. It also requires high resolution.

Second appoach is front tracking in which the front is represented by hypersurface elements (line segments in 2D and triangles in 3D). This approach is best suited to sharp discontinuities.

We apply the front tracking method and the FronTier code to study crystal formation in a generic 3 component reaction-diffusion system. We use front tracking to track the position of the front where there is a discontinuity in solute concentration. We then use finite difference scheme (Crank-Nicolson) to update the concentrations of the reactants and the product which are still in the liquid phase.

The front tracking method treats the moving interface as an interior boundary and applies finite difference method to each subdomain where concentration fields are smooth.

We use the FronTier library to implememnt the front tracking and crystal growth. The functions implemented in the library can be classified as follows: [1]

1. **Initialization:** Initialization functions are capable of initializing the problem parameters as well as geometrical parameters for the computations such dimension, domain, computational grid and boundary conditions. This is done through the input routines. Initialization of the interface is also done through these functions as well as the front velocity initialization.
2. **Query Functions:** Query functions are used to obtain information about the front interface such as vertex coordinates, hypersurface elements (bonds in 2D and triangular surface elements in 3D), access to the manifold (hypersurface), tangents and normals to the surface elements etc.
3. **Propagation Control Functions:** These functions include advancement of the front interface, redistribution and bifurcation.
4. **Front and Subdomain Interaction Functions:** These include the functions which couple the PDE solvers with the front interface functions. These functions can be used to obtain information like the nearest grid points, values of the physical variables in a cell/grid point near the interface etc.

5. **Output and Data Saving Functions:** These functions mainly deal with the data output which is used for visualization of the simulations. The compatible file types include VTK for VisIt, Paraview, Geomview, HDF and GD packages. These functions also have the capability to halt and/or restart the program run from a specific time or time-step.

3 Numerical Method

Consider a reaction-diffusion system given by $nA + mB \longrightarrow C$ and let a seed be already present inside the computational domain. The evolution of concentrations is governed by the following system of equations:

$$\frac{\partial A}{\partial t} = \nabla \cdot (D_A \nabla A) - k_{AB} A^n B^m \tag{9}$$

$$\frac{\partial B}{\partial t} = \nabla \cdot (D_B \nabla B) - k_{AB} A^n B^m \tag{10}$$

$$\frac{\partial C}{\partial t} = \nabla \cdot (D_C \nabla C) + k_{AB} A^n B^m - k \int_F H(C - C_{eq}) \delta(\vec{x} - \vec{x}_f) d\vec{x}_f \tag{11}$$

where $A(\vec{x},t)$, $B(\vec{x},t)$, $C(\vec{x},t)$ are normalized concentrations, D_A, D_B, D_C are diffusion coefficients, $k_{AB} > 0$ is the rate coefficient of homogeneous reaction (liquid phase), $k > 0$ is the rate coefficient of heterogeneous reaction (precipitation), $\vec{x}_f$ is a point on fluid-solid interface and C_{eq} is the equilibrium concentration. $H(\cdot)$ represents the Heaviside step function and $\delta(\cdot)$ represents the dirac-delta function. The integration is taken over the whole fluid-solid interface.

The fluid-solid interface propagates with the normal velocity:

$$v_n(\vec{x}_s) = -\frac{1}{\rho_s} D_C \frac{dC}{dn} \tag{12}$$

where ρ_s is the crystal density and $\frac{dC}{dn}$ is the normal derivative of the concentration $C(\vec{x},t)$.

The FronTier code has the ability to detect if a cell contains liquid phase or solid phase. We use this capability, and for purely liquid phase, we note that $k \int_F H(C - C_{eq}) \delta(\vec{x} - \vec{x}_f) d\vec{x}_f = 0$. Assume that the diffusion coefficients stay constant throughout the liquid phase. Then, for the computational cells containing only the liquid phase, the equations are reduced to:

$$\frac{\partial A}{\partial t} = D_A \nabla^2 A - k_{AB} A^n B^m \tag{13}$$

$$\frac{\partial B}{\partial t} = D_B \nabla^2 B - k_{AB} A^n B^m \tag{14}$$

$$\frac{\partial C}{\partial t} = D_C \nabla^2 C + k_{AB} A^n B^m \tag{15}$$

Any high order finite difference scheme may be used to solve this system of equations. In the present work, we use Crank-Nicolson scheme.

When a cell contains purely solid phase, we assume that there is neither reaction nor diffusion taking place. Thus there is no need to solve the system for the cells containing purely solid phase.

When a cell contains fluid-solid interface, both liquid and solid phases are present inside the cell. At a point on the interface, $k\int_F H(C-C_{eq})\delta(\vec{x}-\vec{x_f})d\vec{x_f} = kH(C-C_{eq})$. To update the concentrations at the grid point of a cell containing the interface, we introduce ghost points in the direction opposite to that of the interface and then solve the system using finite differences. The ghost points are introduced to maintain second order accuracy of the finite difference scheme.

Once the concentrations are updated, we propagate the fluid-solid interface by the methods described by Li et al.[1]. To update the concentrations at a point on the interface, we assume that the solute concentrations at the fluid-solid interface are $A_s = B_s = 0$. Thus, for the $(n+1)$-th time step, the discretized equation for C_s is given by:

$$\frac{C_s^{(n+1)} - C_s^{(n)}}{\Delta t} = \left(D_C \frac{C_{s+h}^{(n+1)} - C_s^{(n+1)}}{h} - kH(C_s^{(n+1)} - C_{eq}) \right) \cdot \frac{2}{h} \tag{16}$$

where h is the spatial step in normal direction. The superscripts denote time step.

Once the concentration of C is updated, it is also necessary to update the concentrations of A and B in the region near the front. To do this, we first approximate the area swept by the moving front. The situation is shown more precisely in the following figure.

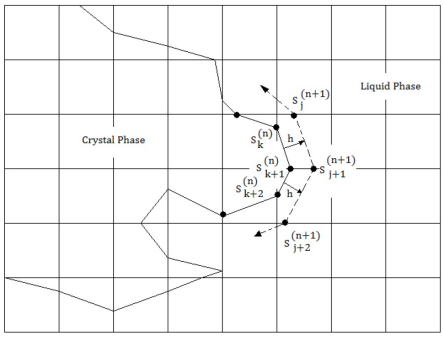

Fig. 1: Advancing the Front and updating concentations

For each segment of the front at time step (n), we approximate the area swept by that segment by the length of the segment times the spatial step in the normal

direction, h. i.e. $\Delta V_k^{(n)} = |S_k^{(n)} - S_{k+1}^{(n)}| \cdot h$. The mass of A and B contained in this area is given by $A \cdot \Delta V_k^{(n)}$ and $B \cdot \Delta V_k^{(n)}$ respectively. A and B in this case are taken to be the interpolated concentrations at the center of the computational cell in which the segment of the front is located. In case the center already lies inside the solid phase, we approximate A and B to be the concentrations at the nearest grid point. We then redistribute this mass equally among the nearest grid points at time step $(n+1)$.

4 Numerical Results

In this section, we present the numerical results which show the effects of different parameters on the crystal growth. The parameters which control the reaction-diffusion system described by equations (9) to (11) are D_A, D_B, D_C and k_{AB}, k.

We set the computational domain to be the square $[0,1] \times [0,1]$. The boundary conditions used for testing are $A(x,0,t) = B(x,1,t) = 0$ and $A(x,1,t) = B(x,0,t) = 1$.

4.1 Effects of k_{AB} and k

We first explore the effects of k_{AB} and k on the crystal growth. Initial concentrations are assumed to be uniformy distributed along the y-axis.

It can be observed from the following tests that the dendritic growth is pronounced when k is high. k_{AB} has negligible effect on the dendritic growth. It will also be observed that in general, the direction in which dendrites grow is controlled by $\frac{D_A}{D_B}$. This point will be further explored in the next section.

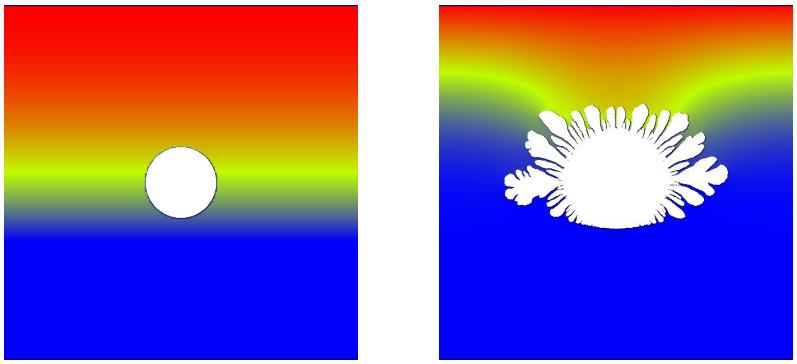

(a) $t = 0$ (b) $t = 2.755$

Fig. 2: Parameters are $k_{AB} = 150$, $k = 800$ and $D_A = 0.3$, $D_B = 0.7$, $D_C = 0.5$

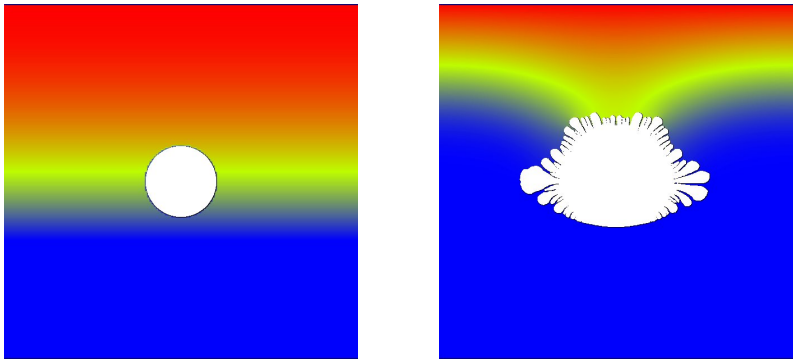

(a) $t = 0$ (b) $t = 2.755$

Fig. 3: Parameters are $k_{AB} = 1500$, $k = 200$ and $D_A = 0.3$, $D_B = 0.7$, $D_C = 0.5$

4.2 Effect of the diffusivities

As mentioned in the previous section, the direction in which the dendrites grow is controlled by the value of $\frac{D_A}{D_B}$. The effects are explored in this section. The initial conditions vary for each simulation. However, initial conditions are found to have negligible effect on the direction of growth.

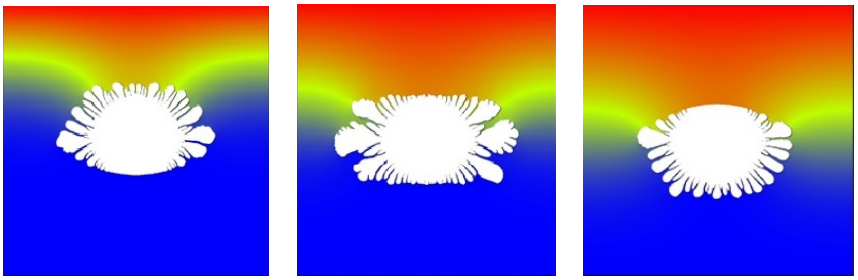

(a) $D_A = 0.3$, $D_B = 0.7$ (b) $D_A = 0.5$, $D_B = 0.5$ (c) $D_A = 0.7$, $D_B = 0.3$

Fig. 4: Parameters are $k_{AB} = 150$, $k = 800$ and $D_C = 0.5$ Each image is taken at $t = 2.68$

4.3 Effect of the Damkohler Number

The Damkohler Number, d, is defined by $d = \frac{kL}{D_C}$ [1, 2] where k is the heterogeneous reaction constant, L is the characteristic length and D_C is the diffusion

coefficient for the product C. Damkohler number is closely tied with the dendritic growth of the crystal. High Damkohler number produces high dendritic structure and vice-versa. In this section, we provide numerical results which show that the dendritic growth in a Reaction-Diffusion System for $A+B \longrightarrow C$ occurs only when the Damkohler number is higher than a threshold value. In most of our simulations, the threshold was in the range of 60 to 80. Although it is diffcult to predict the exact value of the threshold, we mention that traces of dendritic structures started to appear for $d = 60$ and they were well formed for $d = 80$. For lower Damkohler numbers, the crystal growth was smooth without any dendrites. The direction of the growth was still controlled by $\frac{D_A}{D_B}$. The initial shape of the seed had no effect on the threshold value.

The computational domain is $[0,1] \times [0,1]$. Reactants A and B are initially separated at $y = 0.5$. Other parameters are as follows: $k_{AB} = 1500$, $D_A = 0.3$, $D_B = 0.7$. We wish to mention that the simulations were carried out for a range of Damkohler Numbers, in particular for $d = 0.1, 0.5, 1, 5, 10, 20, 40, 60, 80, 160$. For small values of d, the crystal growth was not qualitatively different, the only signi

cant difference being the amount of growth in a given time. We also carried out the simulations for a range of values of D_A and D_B. Numerical results showed difference in the direction of crystal growth.

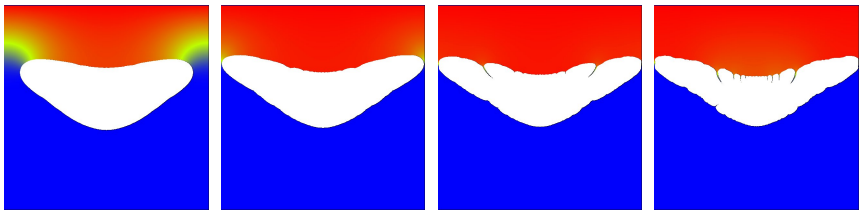

(a) $d = 20$ (b) $d = 40$ (c) $d = 60$ (d) $d = 80$

Fig. 5: Effects of the Damkohler Number. Parameters are $k_{AB} = 1500$, $D_A = 0.3$ and $D_B = 0.7$. Each image is taken at $t = 2.57$. Initial seed is circular.

4.4 Effect of the equilibrium concentration

The supersaturation theory asserts that the deposition of mass occurs only when $C_s > C_{eq}$ where C_s is the concentration of C at a point on the fluid-solid interface and C_{eq} is the equilibrium concentration. The theory also asserts that once the concentration C attains the equilibrium concentration, the deposition occurs instantaneously. It is natural to expect that this process will have effect on the dendritic growth. This is confirmed by the following numerical results. Lower equilibrium concentration produces more dendritic growth and vice-versa, when all other parameters are held constant. Parameters used are $k_{AB} = 1500$, $k = 100$, $D_A = 0.3$, $D_B = 0.7$, and $D_C = 0.5$. Other computational setup is the same as previous sections.

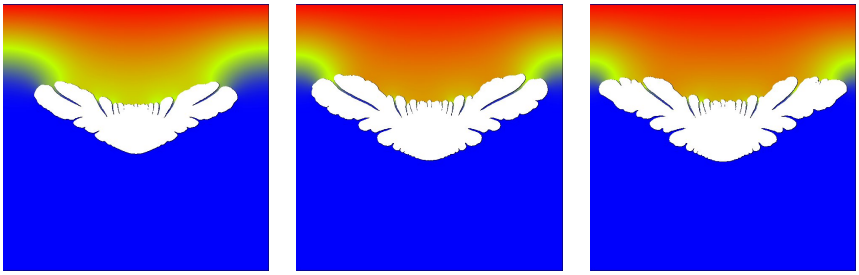

(a) $C_{eq} = 0.1$ (b) $C_{eq} = 0.01$ (c) $C_{eq} = 0.001$

Fig. 6: Effects of the Equilibrium Concentration. Parameters are $k_{AB} = 1500$, $k = 100$, $D_A = 0.3$, $D_B = 0.7$, and $D_C = 0.5$. Each image is taken at $t = 2.629$. Initial seed is circular.

5 Summary and Conclusions

In the present work involving the crystal growth in a reaction-diffusion system containing three components, we examined the effects of parameters D_A, D_B, D_C and k_{AB}, k. We found that the dendritic growth is controlled predominantly by the heterogeneous reaction constant k, and the homogeneous reaction constant k_{AB} has no effect on the dendrites. We also observed that the direction in which the dendrites grow is controlled by $\frac{D_A}{D_B}$. Numerical simulations show that the Damkohler number produces dendritic growth only if it's value is higher than some threshold. The threshold for the tests done in the presenst study appears to be in the range of $d = 60$ to $d = 80$. The equilibrium concentration, C_{eq} also has effect on the dendrites with lower C_{eq} being responsible for higher dendritic growth and vice-versa.

Acknowledgements This work is supported in part by the US Army Research Office under the award W911NF-14-1-0428 and the ARO-DURIP Grant W911NF-15-1-0403. We would also like to thank Roman Samulyak and Yangang Liu for their suggestions. Also, thanks to Yijing Hu for helpful discussions and earlier work on the problem of crystal growth.

References

1. Study of crystal growth and solute precipitation through front tracking method, *Acta Mathematica Scientia, Volume 30, Issue 2, March 2010, Pages 377-390,* Xiaolin Li, James Glimm, Xiangmin Jiao, Charles Peyser, Yanhong Zhao
2. Numerical simulations of phase transition problems with explicit interface tracking, *Chemical Engineering Science 128(2015) 92-108,* Yijing Hu, Qiangqiang Shi, Valmor F. De Almeida, Xiaolin Li
3. Hybrid Simulations of Reaction-Diffusion Systems in Porous Media, *SIAM J. Sci. Comput. 30 2799 (2008),* A. M. Tartakovsky, D. M. Tartakovsky, T. D. Scheibe, and P. Meakin

4. Reaction-Diffusion Cellular Automata Model for the Formation of Liesegang Patterns, *Phys. Rev. Lett. 72, 1384-1387 (1994),* B. Chopard, P. Luthi and M. Droz
5. Wilhelm Ostwald, *Lehrbuch der Allgemeinen Chemie II/2,* W. Engelmann, Leipzig (1896-1902)
6. Patterns Produced by Precipitation at a Moving Reaction Front, *Phys. Rev. Lett. 57, 275-278 (1986),* G. T. Dee
7. Measurements and Hypothesis on Periocic Precipitation Processes, *J. Phys. Chem. 91, 6300-6308 (1987),* M. E. LeVan and J. Ross
8. Derivation of the Matalon-Packter law for Liesegang paterns, *J. Chem. Phys. 109, 9479-9486 (1998),* T. Antal, M. Droz, J. Magnin, Z. Racz and M. Zrnyi
9. The Liesegang Phenomenon. I. Sol Protection and Diffusion, *J. Colloid Sci. 10, 46-61 (1955),* R. Matalon and A. Packter
10. Pattern Formation in a New Class of Precipitation Reactions, *Ph.D. Thesis, Peter Hantz,* UNIVERSITÉ DE GENÈVE
11. Chemistry and Crystal Growth, *Angew. Chem. Int. Ed. Engl. 33, 143-162 (1994),* Jurg Hulliger
12. Dendrites, Viscous Fingers, and the Theory of Pattern Formation, *Science 243, 1150-1156 (1989),* J. S. Langer
13. Competition between kinetic and surface tension anisotropy in dendritic growth, *Eur. Phys. J. B 16, 337-344 (2000),* T. Ihle
14. Diffusion-Limited Aggregation: A Model for Pattern Formation, *Physics Today 53, 36-41 (2000),* Thomas C. Halsey
15. Mathematical Analysis of the Formation of Periodic Precipitates, *J. Colloid Sci. 5, 85-97 (1950),* C. Wagner
16. Periodic Precipitation Patterns in the Presence of Concentration Gradients 1., *J. Phys. Chem. 86, 4078-4087 (1982),* Stefan C. Muller, Shoichi Kai and John Ross
17. The Formation of Liesegang Rings as a Periodic Coagulation Phenomenon, *Journal of the Chemical Society 1928/II, 2714-2727 (1928),* Ernest S. Hedges and Rosalind V. Henley
18. Mechanism of chemical instability for periodic precipitation phenomena, *J. Chem. Phys. 60, 3458-3465 (1974),* Michael Flicker and John Ross
19. The Concentration Distribution in the Gel before the Periodic Precipitation, *Memoirs of the Faculty of Science, Kyushu University, Series C Chemistry, 5, 33-42 (1962),* Hiroshige Higuchi and Ryohei Matura
20. Nucleation and Spinodal Decomposition, *Solid State Phenomena 56, 67-106 (1997),* L. Granasy
21. Phase Transitions and Critical Phenomena, *vol. 8, Academic Press, London (1989),* C. Domb and J. L. Lebowitz (editors)
22. Formation of Liesegang Patterns, *Physica A 274, 50-59 (1999),* Zoltan Racz
23. Pattern formation induced by ion-selective surfaces: Models and simulations, *J. Chem. Phys. 123, 034707 (2005),* Szabolcs Horvt and Pter Hantz
24. Properties of the reaction front in an $A+B \longrightarrow C$ type reaction-diffusion process, *Physical Review A 1988, Volume 38, Number 6: 3151-3154,* L. Gal and Z. Racz
25. Properties of the asymptotic $nA+mB \longrightarrow C$ reaction-diffusion fronts, *Eur. Phys J. B 17 (2000): 673-678,* J. Magnin
26. Dynamic multiscaling of the recation-diffusion front for $mA+nB \longrightarrow C$, *Physical Review E, October 1995, Volume 52, Number 4,* S. Cornell, Z. Koza and M. Droz
27. Reaction front for $A+B \longrightarrow C$ diffusion-reaction systems with initially separated reactants, *Physical Review A, July 1992, Volume 46, Number 2,* H. Larralde, M. Araujo, S. Havlin and H. Stanley
28. Steady-State Reaction-Diffusion Front Scaling for $mA+nB \longrightarrow C$, *Physical Review Letters, June 1993, Volume 70, Number 24,* S. Cornell and M. Droz
29. Asymptotic behaviour of initially separated $A+B_{(static)} \longrightarrow C$ reaction-diffusion systems, *Physica A 240 (1997) 622-634,* Z. Koza
30. Reaction-Diffusion fronts in systems with concentration-dependent diffusivities, *Physical Review E 74, 036103 (2006),* P. Polanowski and Z. Koza

31. Reaction fronts in reversible $A + B \rightleftharpoons C$ reaction-diffusion systems, *Physica A 330 (2003) 160-166,* Z. Koza
32. Reversible and irreversible reaction fronts in two competing reaction system, *Nuclear Instruments and Methods in Physica Research B 186 (2002) 161-165,* M. Sinder, H. Taitelbaum, J. Pelleg
33. Asymptotic expansion for reversible $A + B \longleftrightarrow C$ reaction-diffusion process, *Physical Review E 66, 011103 (2002),* Z. Koza
34. The Long-time Behavior of Initially Separated $A + B \longrightarrow C$ Reaction-Diffusion Systems with Arbitrary Diffusion Constants, *J. Stat. Phys. 85, 179-191(1996),* Z. Koza
35. Some Properties of the $A + B \longrightarrow C$ Reaction-Diffusion System with Initially Separated Components, *Journal of Statistical Physics, Vol. 65, Nos. 5/6, 1991,* H. Taitelbaum, S. Havlin, J. Kiefer, B. Trus, and G. Weiss
36. Numerical analysis of reversible $A + B \longleftrightarrow C$ reaction-diffusion systems, *Eur. Phys. J. B 32, 507-511(2003),* Z. Koza
37. Simulation study of reaction fronts, *Physical Review A, December 1990, Volume 42, Number 12,* Z. Jiang and C. Ebner
38. Refined simulations of the reaction front for diffusion-limited two-species annihilation in one dimension, *Physical Review E, May 1995, Volume 51, Number 5,* S. Cornell
39. Role of fluctuations for inhomogeneous reaction-diffusion phenomena, *Physical Review A, Volume 44, Number 8, Oct. 1991,* S. Cornell, M. Droz, B. Chopard
40. A Front-Tracking Method for Viscous, Incompressible, Multi-fluid Flows, *Journal of Computational Physics 100, 25-37 (1992),* Salih Ozen Unverdi, Gretar Tryggvason
41. Numerical simulation of dendritic solidification with convection: Two-Dimensional Geometry, *Journal of Computational Physics, Volume 180, Issue 2, 10 August 2002, Pages 471-496,* Nabeel Al-Rawahi, Gretar Tryggvason
42. Numerical simulation of dendritic solidification with convection: Three-dimensional flow, *Journal of Computational Physics, Volume 194, Issue 2, 1 March 2004, Pages 677-696,* Nabeel Al-Rawahi, Gretar Tryggvason
43. Front tracking for gas dynamics, *Journal of Computational Physics, Volume 62, Issue 1, January 1986, Pages 83-110,* I.-L Chern, J. Glimm, O. Mcbryan, B. Plohr, S. Yaniv
44. A simple package for front tracking, *Journal of Computational Physics 213:613-628, 2006,* Jian Du, Brian Fix, James Glimm, Xicheng Jia, Xiaolin Li, Yunhua Li, and Lingling Wu
45. A level set simulation of dendritic solidification with combined features of front-tracking and fixed-domain methods, *Journal of Computational Physics, 211:36-63, 2006,* Lijian Tan and Nicholas Zabaras
46. Front tracking in two and three dimensions, *Comput. Math. Appl., 35(7):1-11, 1998,* J. Glimm, M. J. Graham, J. W. Grove, X.-L. Li, T. M. Smith, D. Tan, F. Tangerman, and Q. Zhang
47. Frontier and applications to scientific and engineering problems, *Proceedings of International Congress of Industrial and Applied Mathematics, pages 1024507 - 1024508, 2008,* W. Bo, B. Fix, J. Glimm, X. L. Li, X. T. Liu, R. Samulyak, and L. L. Wu
48. Diamond crystsal growth by plasma chemical vapor deposition, *Journal of Applied Physics, 63:1744-1748, 1988,* C. P. Chang, D. L. Flamm, D. E. Ibbostson, and J. A. Mucha
49. Precipitation and dissolution of reactive solutes in fractures, *Water Resources Research, 34:457-470, 1998,* Peter Dijk and Brian Berkowitz
50. Simulation of dissolution and precipitation in porous media, *J. Geophys. Res., 108:2505, 2003,* Q. Kang, D. Zhang, and S. Chen
51. Numerical modeling of ice deposition, *Journal of the Atmospheric Sciences, 28:226-237, 1970,* L. R. Koenig
52. An experimental investigation of nonaqueous phase liquid dissolution in saturated subsurface systems: Steady state mass transfer rates, *Water Resources Research, 28:2691-2705, 1992,* Susan E. Powers, Linda M. Abriola, and Walter J. Weber JR